Polyunsaturated fatty acid biosynthesis pathway determines ferroptosis sensitivity in gastric cancer

Ji-Yoon Lee[a,b,1], Miso Nam[c,1,2], Hye Young Son[d,1], Kwangbeom Hyun[a], Seo Young Jang[c,e], Jong Woo Kim[b,f], Min Wook Kim[b], Youngae Jung[c], Eunji Jang[g], Seon-Jin Yoon[h], Jungeun Kim[g], Jihye Kim[g], Jinho Seo[i], Jeong-Ki Min[e,j], Kyoung-Jin Oh[b,f], Baek-Soo Han[f,k], Won Kon Kim[b,f], Kwang-Hee Bae[b,f,l], Jaewhan Song[m], Jaehoon Kim[a], Yong-Min Huh[d,g,l,n,3], Geum-Sook Hwang[c,e,3], Eun-Woo Lee[b,3], and Sang Chul Lee[b,3]

[a]Department of Biological Sciences, Korea Advanced Institute of Science and Technology, 34141 Daejeon, Korea; [b]Metabolic Regulation Research Center, Korea Research Institute of Bioscience and Biotechnology (KRIBB), 34141 Daejeon, Korea; [c]Integrated Metabolomics Research Group, Western Seoul Center, Korea Basic Science Institute, 03759 Seoul, Korea; [d]Severance Biomedical Science Institute, Yonsei University College of Medicine, 03722 Seoul, Korea; [e]Department of Chemistry and Nano Science, Ewha Woman's University, 03760 Seoul, Korea; [f]Department of Functional Genomics, University of Science and Technology, 34141 Daejeon, Korea; [g]MediBio-Informatics Research Center, Novomics Co., Ltd., 07217 Seoul, Korea; [h]Department of Biochemistry and Molecular Biology, Yonsei University College of Medicine, 03722 Seoul, Korea; [i]Environmental Diseases Research Center, KRIBB, 34141 Daejeon, Korea; [j]Biotherapeutics Translational Research Center, KRIBB, 34141 Daejeon, Korea; [k]Biodefense Research Center, KRIBB, 34141 Daejeon, Korea; [l]Yonsei University Health System (YUHS)-KRIBB Medical Convergence Research Institute, 03722 Seoul, Korea; [m]Department of Biochemistry, College of Life Science and Biotechnology, Yonsei University, 03722 Seoul, Korea; and [n]Department of Radiology, Severance Hospital, Yonsei University College of Medicine, 03722 Seoul, Korea

Edited by Benjamin F. Cravatt, Scripps Research Institute, La Jolla, CA, and approved November 5, 2020 (received for review April 10, 2020)

Ferroptosis is an iron-dependent regulated necrosis mediated by lipid peroxidation. Cancer cells survive under metabolic stress conditions by altering lipid metabolism, which may alter their sensitivity to ferroptosis. However, the association between lipid metabolism and ferroptosis is not completely understood. In this study, we found that the expression of elongation of very long-chain fatty acid protein 5 (ELOVL5) and fatty acid desaturase 1 (FADS1) is up-regulated in mesenchymal-type gastric cancer cells (GCs), leading to ferroptosis sensitization. In contrast, these enzymes are silenced by DNA methylation in intestinal-type GCs, rendering cells resistant to ferroptosis. Lipid profiling and isotope tracing analyses revealed that intestinal-type GCs are unable to generate arachidonic acid (AA) and adrenic acid (AdA) from linoleic acid. AA supplementation of intestinal-type GCs restores their sensitivity to ferroptosis. Based on these data, the polyunsaturated fatty acid (PUFA) biosynthesis pathway plays an essential role in ferroptosis; thus, this pathway potentially represents a marker for predicting the efficacy of ferroptosis-mediated cancer therapy.

ferroptosis | lipid peroxidation | ELOVL5 | FADS1 | arachidonic acid

Ferroptosis, an iron-dependent type of necrotic cell death, is an emerging cell death pathway that is associated with several pathological conditions, including ischemia-reperfusion (I/R) injury, neurodegeneration, and cancer (1–4). In the normal state, polyunsaturated fatty acids (PUFAs) are frequently oxidized by lipoxygenases such as 12/15-lipoxygenase but immediately reduced by the enzyme glutathione peroxidase 4 (GPX4) and its cofactor glutathione (GSH) (2, 5). However, when GPX4 is inhibited or GSH is depleted, lipid peroxides accumulate in cells, leading to lipid peroxidation-induced cell death, which is called ferroptosis (1, 2, 6). Several radical-trapping antioxidants (RTAs), such as ferrostatin-1 and liproxstatin-1, which trap lipid peroxyl radicals, have been identified as ferroptosis inhibitors (1, 7). These inhibitors exert a protective effect on mouse models of I/R-induced renal failure, liver injury, and doxorubicin-induced cardiomyopathy, suggesting a critical role for ferroptosis in various diseases (7–9).

Since intracellular GSH is synthesized from cysteine, the maintenance of certain levels of cysteine is critical for protecting cells from ferroptosis. Cysteine homeostasis is supported from outside the cell through system x_c^-, a cystine/glutamate antiporter that imports cystine (the oxidized form of cysteine). Erastin was first identified as a ferroptosis inducer that inhibits system x_c^- (1, 10). Sorafenib also inhibits system x_c^- and induces ferroptosis, particularly in hepatocarcinoma cells (10–12). In addition, cysteine is synthesized from methionine by the cystathionine β-synthase (CBS) enzyme and cystathionine γ-lyase (CTH) via the transsulfuration pathway. The inhibition of transsulfuration pathways has also been shown to trigger ferroptosis in certain types of cells (13, 14). According to a recent study, cancer cells differentially express xCT, the regulatory component of the system x_c^-, and CBS, rendering them dependent on the x_c^- system or the transsulfuration pathway for the maintenance of intracellular cysteine pools (15). The transsulfuration pathway may protect cells from ferroptosis when cysteine homeostasis is not fully

Significance

Phosphatidylethanolamine (PE)-linked arachidonic acid (AA) and adrenic acid (AdA) are well-known substrates for lipid peroxidation, which are indispensable for ferroptosis, an iron-dependent regulated necrosis. However, how cells differentially regulate the intracellular pools of AA and AdA is not fully understood. Here, elongation of very long-chain fatty acid protein 5 (ELOVL5) and fatty acid desaturase 1 (FADS1) are differentially expressed in gastric cancer cells, discriminating the cellular susceptibility to ferroptosis. Biochemical and lipidomics analyses support the hypothesis that ELOVL5 and FADS1 are required to maintain intracellular levels of AA and AdA and promote ferroptosis. Our study highlights the biosynthesis of AA and AdA by ELOVL5 and FADS1 as a critical checkpoint in the ferroptosis pathway.

Author contributions: J.-Y.L., M.N., H.Y.S., K.H., K.-J.O., B.-S.H., W.K.K., K.-H.B., J. Song, Jaehoon Kim, Y.-M.H., G.-S.H., E.-W.L., and S.C.L. designed research; J.-Y.L., M.N., H.Y.S., K.H., S.Y.J., J.W.K., M.W.K., Y.J., E.J., S.-J.Y., Jungeun Kim, Jihye Kim, J. Seo, J.-K.M., G.-S.H., E.-W.L., and S.C.L. performed research; J.-Y.L., M.N., H.Y.S., S.Y.J., Y.J., Y.-M.H., G.-S.H., E.-W.L., and S.C.L. analyzed data; and J.-Y.L., M.N., H.Y.S., Y.-M.H., G.-S.H., E.-W.L., and S.C.L. wrote the paper.

Competing interest statement: Y.M.H. is a founder of Novomics Co., Ltd. and E.J., J.K., and Jihye Kim are full-time employees of Novomics Co., Ltd.

The authors declare no competing interest.

This article is a PNAS Direct Submission.

[1]J.-Y.L., M.N., and H.Y.S. contributed equally to this work.

[2]Present address: Department of Molecular and Human Genetics, Baylor College of Medicine, Houston, TX 77030.

[3]To whom correspondence may be addressed. Email: ymhuh@yuhs.ac, gshwang@kbsi.re.kr, ewlee@kribb.re.kr, or lesach@kribb.re.kr.

This article contains supporting information online at https://www.pnas.org/lookup/suppl/doi:10.1073/pnas.2006828117/-/DCSupplemental.

First published December 7, 2020.

supported by cancer cells under certain conditions, including hypoxia. The direct inhibition of GPX4 by specific inhibitors, such as RSL3 and ML210, also rapidly induces ferroptotic cell death (16, 17). Interestingly, mitochondria play a key role in cysteine deprivation-induced ferroptosis, whereas they are dispensable for GPX4 inhibition-induced ferroptosis (18).

Most cancer cells, including renal cell carcinoma, melanoma, hepatocarcinoma, and lung cancer, have been reported to undergo ferroptosis upon the inhibition of GPX4 or system x_c^-. Therapy-resistant cancer cells have recently been reported to exhibit increased susceptibility to ferroptosis, possibly due to their increased lipid metabolism via the TGF-ZEB1 pathway (19, 20). Since ferroptosis is induced by the peroxidation of PUFAs, the regulation of lipid metabolism is a crucial determinant of ferroptosis sensitivity. A phospholipidomic analysis revealed that specific phospholipids, such as phosphatidylethanolamine (PE)-conjugated arachidonic acid (AA) and adrenic acid (AdA), are preferentially oxidized by lipoxygenases (21, 22). The crucial roles of PE-conjugated AA have also been identified in a study showing that phosphatidylethanolamine-binding protein 1 (PEBP1), which binds to lipoxygenase and free AA, regulates ferroptotic cell death (22). In addition, long-chain acyl-CoA synthetase 4 (ACSL4), which esterifies AA and AdA into acyl-CoA to produce AA- or AdA-containing PE, is essential for ferroptosis (21). ACSL4 expression is frequently lost in luminal-type breast cancer cells, leading to ferroptosis resistance, whereas basal-type cells express ACSL4 and undergo ferroptosis upon GPX4 knockout (KO) and RSL3 treatment (21).

In the present study, we investigated the expression of genes related to lipid and iron metabolism using a panel of gastric cancer cells (GCs) with different sensitivities to ferroptosis to identify a new protein that regulates ferroptosis. As a result, two enzymes involved in PUFA biosynthesis, ELOVL5 and FADS1, are determining factors regulating ferroptosis. Cells expressing these enzymes display increased levels of AA and AdA and are sensitive to ferroptosis. In contrast, cells with low expression of these enzymes are resistant to ferroptosis, but the sensitivity of these cells to ferroptosis is increased by the addition of exogenous AA. Based on these results, the PUFA biosynthesis pathway plays an essential role in ferroptosis in cancer cells.

Results

Mesenchymal-Type GCs, but Not Intestinal-Type GCs, Are Sensitive to Ferroptosis. GCs with a mesenchymal or stromal gene signature exhibit a poor response to chemotherapy, while intestinal-type GCs are generally sensitive to chemotherapy (23–25). Therefore, we wondered whether the sensitivity to ferroptosis also depends on the type of GCs. The gene signatures of a panel of GCs were confirmed using a microarray and categorized into mesenchymal-, intestinal-, and mixed-type GCs using the previously described nonnegative matrix factorization (NMF) clustering method (24) to test this hypothesis (Fig. 1*A*). By analyzing the viability of the GCs upon treatment with RSL3, a GPX4 inhibitor, mesenchymal-type GCs, including Hs746T, SNU-484, SNU-668, YCC-16, and SNU-216 cells, are highly sensitive to ferroptosis (Fig. 1*A*). In contrast, intestinal-type GCs, including MKN-45, NCI-N87, SNU-601, SNU-719, and YCC-7 cells, are resistant to RSL3-induced ferroptosis (Fig. 1*A*). Furthermore, the sensitivity to RSL3 was significantly correlated with mesenchymal gene signatures calculated from stem-like or stromal score of each GC line, implying that chemoresistant GCs might be highly sensitive to ferroptosis (Fig. 1 *B* and *C* and Dataset S1) (24, 26). In addition, another GPX4 inhibitor, ML210, selectively reduced the viability of Hs746T and SNU-484 cells (Fig. 1*D*). Ferrostatin-1 and liproxstatin-1, two ferroptosis inhibitors, almost completely reversed RSL3- or ML210-induced cell death, whereas the pan-caspase inhibitor zVAD-fmk or the RIPK1 inhibitor necrostatin-1 did not (Fig. 1 *E*–*G*) (1, 7). Thus, RSL3 and ML210 selectively induce ferroptosis in mesenchymal-type GCs.

We next wondered whether the sensitivity of cells to GPX4 inhibitors was similar to their sensitivity to other ferroptotic stimuli, such as GSH depletion. Consistent with previous reports, we observed a depletion of intracellular GSH levels when cells were cultured with cysteine/methionine-deficient medium (*SI Appendix*, Fig. S1*A*) (13, 15, 18, 27, 28). As the GSH levels decreased, cell death increased in two mesenchymal-type GCs (*SI Appendix*, Fig. S1 *B* and *C*). The decrease in cell viability and increase in lactate dehydrogenase (LDH) release were markedly rescued in the presence of ferrostatin-1, suggesting that GSH depletion mainly induces ferroptotic cell death (*SI Appendix*, Fig. S1 *B* and *C*). However, intestinal-type GCs, such as NCI-N87 and SNU-719 cells, were also resistant to cysteine/methionine deprivation-induced ferroptosis, despite the comparable depletion of GSH (*SI Appendix*, Fig. S1 *B* and *C*).

ELOVL5 and FADS1 Expression Is Up-Regulated in Mesenchymal-Type GCs. These observations prompted us to identify the key factors that determine ferroptosis sensitivity by comparing gene expression levels between mesenchymal- and intestinal-type GCs. Since RSL3 directly binds to and inhibits GPX4 activity, we focused on the genes associated with lipid and iron metabolism rather than GSH metabolism and identified several genes whose expression was significantly up-regulated or down-regulated in mesenchymal-type GCs compared with intestinal-type GCs (Fig. 2*A* and Datasets S2 and S3). Among these genes, *ELOVL5* and *FADS1*, which are involved in the generation and utilization of long-chain PUFAs, were expressed at higher levels in all mesenchymal-type GCs than in intestinal-type GCs (Fig. 2 *A* and *B* and *SI Appendix*, Fig. S2*A*). ELOVL5 and FADS1 are enzymes required for the generation of AA (C20:4) and AdA (C22:4) from linoleic acid (LA, C18:2) (Fig. 2*C*). Given that AA and AdA are the most susceptible PUFAs to lipid peroxidation (21), certain levels of these enzymes might be required for lipid peroxidation and ferroptosis.

We next sought to evaluate the levels of the ELOVL5 and FADS1 proteins in various GCs by performing a Western blot analysis. When we employed two ELOVL5 antibodies, one antibody detected bands at ∼40 kDa, which is similar to the expected molecular weight of ELOVL5 (35 kDa) based on its amino acid (aa) sequence of 299 aa (*SI Appendix*, Fig. S2*B*). However, these bands were observed in all intestinal-type GCs and one mesenchymal-type GC line (*SI Appendix*, Fig. S2*B*). When we validated the results using an ELOVL5 siRNA pool consisting of four independent siRNAs, however, these bands were not depleted by the siRNA treatment, indicating that these bands did not represent the ELOVL5 protein (*SI Appendix*, Fig. S2 *C* and *D*). Surprisingly, we observed a band with a molecular weight greater than 180 kDa in all mesenchymal-type GCs, but not in intestinal-type GCs, using both antibodies (*SI Appendix*, Fig. S2*B*). The >180-kDa band might be the aggregated form of the ELOVL5 proteins, as suggested in a previous study showing that this protein aggregates during boiling (29). Similarly, we could detect ELOVL5 protein at ∼30 kDa in all mesenchymal-type GCs using unboiled lysates (Fig. 2*D*). In addition, both the >180- and 30-kDa bands disappeared after treatment with the pool of ELOVL5 siRNAs and were absent in ELOVL5 KO cells, suggesting that these bands represent the actual ELOVL5 protein (*SI Appendix*, Fig. S2 *C*–*I*).

Next, the specificity of five antibodies against FADS1 was tested. Several FADS1 antibodies recognized proteins with sizes of ∼55 kDa, which is the predicted molecular weight of FADS1 consisting of 501 amino acids (*SI Appendix*, Fig. S2*J*). However, siRNA-mediated knockdown experiments implied that only the antibody from Atlas Antibodies recognized the FADS1 proteins (*SI Appendix*, Fig. S2 *J*–*M*). Furthermore, the band detected by the Atlas antibody was no longer visible in lysates from FADS1 KO cells, confirming the specificity of this FADS1 antibody

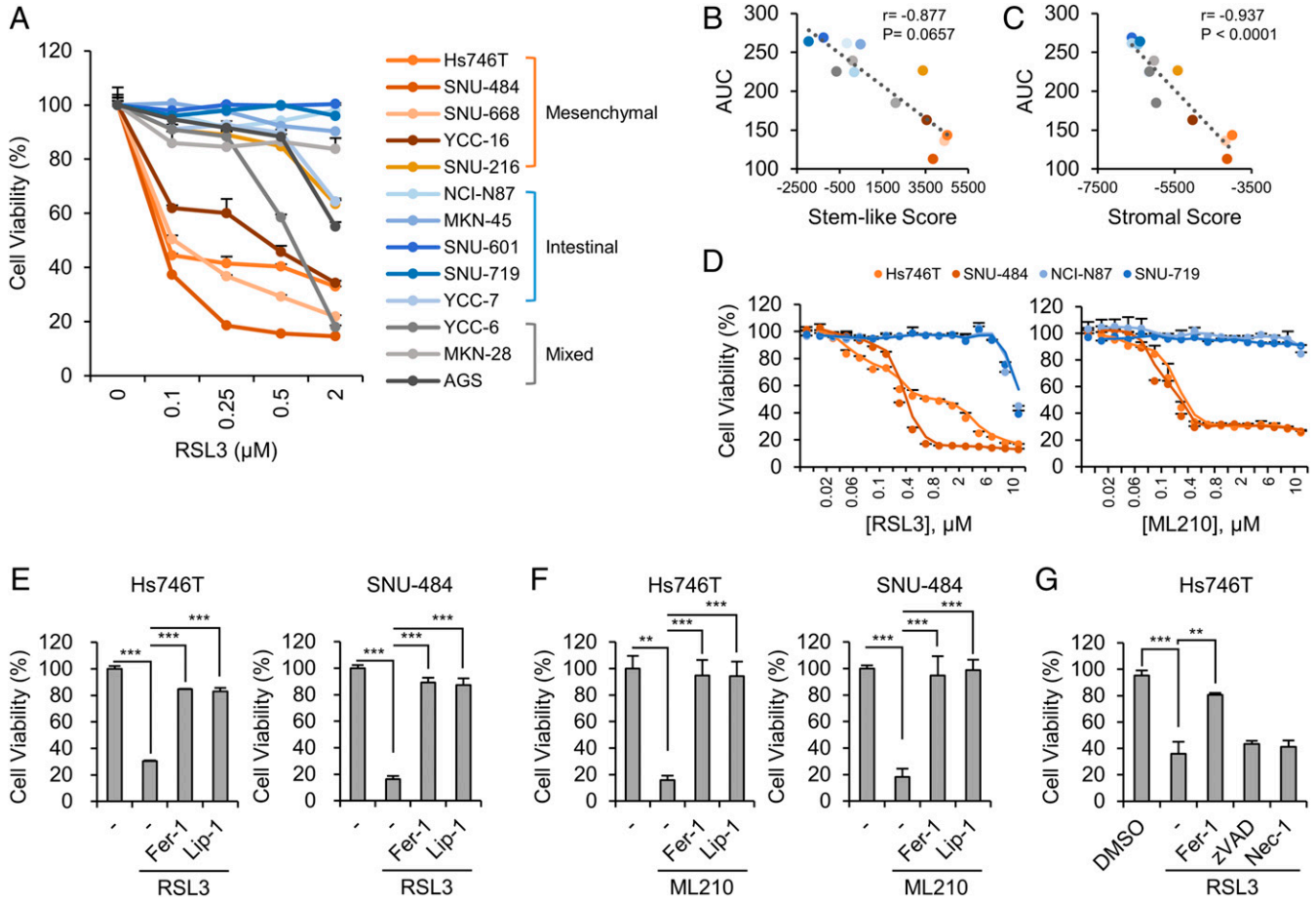

Fig. 1. Mesenchymal-type gastric cancer cells (GCs) are sensitive to ferroptotic cell death. (*A*) Relative viability of GCs treated with RSL3 (0.1 to 5 μM) for 24 h. Data are the means ± SD ($n = 3$ independent experiments). (*B* and *C*) Scatterplots between area under curve (AUC) for RSL3 in A and mesenchymal (*B*) or stromal (*C*) scores in GCs. Dots indicate each GC line, and Pearson's correlation coefficients and *P* values are shown in graphs. (*D*) Relative viability of mesenchymal-type (Hs746T and SNU-484) and intestinal-type (NCI-N87 and SNU-719) GCs treated with RSL3 and ML210 (0.01 to 10 μM) for 24 h. Data are the means ± SD ($n = 3$ independent experiments). (*E*) Relative viability of Hs746T and SNU-484 cells treated with 1 μM RSL3 in the presence and absence of ferrostatin-1 (Fer-1, 1 μM) or liproxstatin-1 (Lip-1, 200 nM). Data are the means ± SD ($n = 3$ independent experiments, with $^{***}P < 0.001$ according to two-sided Student's *t* tests). (*F*) Relative viability of Hs746T and SNU-484 cells treated with 5 μM ML210 and inhibitors. Data are the means ± SD ($n = 3$ independent experiments, with $^{**}P < 0.01$ and $^{***}P < 0.001$ according to two-sided Student's *t* tests). (*G*) Relative viability of Hs746T cells treated with zVAD-fmk (zVAD, 10 μM), necrostatin-1 (Nec-1, 30 μM), Fer-1 (1 μM), and/or RSL3 (1 μM). Data are the means ± SD ($n = 3$ independent experiments, with $^{**}P < 0.01$ and $^{***}P < 0.001$ according to two-sided Student's *t* tests).

(*SI Appendix*, Fig. S2 *N* and *O*). Using this antibody, FADS1 proteins were detected in all mesenchymal-type GCs, but not in intestinal-type GCs. Collectively, mesenchymal cells express the ELOVL5 and FADS1 mRNAs and proteins at higher levels, while intestinal-type cells do not express these enzymes.

Mesenchymal-Type GCs Contain More Ferroptosis-Related Lipids Than Intestinal-Type GCs. We conducted a lipid profiling analysis using liquid chromatography tandem mass spectrometry (LC-MS/MS) to examine whether the increased levels of ELOVL5 and FADS1 are indeed associated with the levels of related metabolites. Interestingly, AA (C20:4), AdA (C22:4), and PE (18:0/22:4) were among the top four significantly enriched PUFAs detected in the mesenchymal-type cells compared to intestinal-type cells (Fig. 2*E* and *SI Appendix*, Fig. S3). In addition, the levels of PE- and phosphatidylcholine (PC)-linked fatty acids with a long-chain length and high degree of unsaturation were increased in mesenchymal-type GCs (*SI Appendix*, Fig. S3). In contrast, most lysophospholipids (lysoPLs), phosphatidylglycerol (PG), phosphatidylinositol (PI) were more abundant in intestinal-type GCs than in mesenchymal-type GCs (*SI Appendix*, Fig. S3). Since n-6 long-chain PUFAs such as AA (C20:4) and AdA (C22:4) are synthesized from essential fatty acids such as LA (C18:2), we focused on the levels of free fatty acids in the n-6 PUFA biosynthesis pathway (Fig. 2*C*). Notably, AA (C20:4) and AdA (C22:4) were detected at higher levels in most mesenchymal-type GCs than in intestinal-type GCs, but significant differences in the levels of LA (C18:2) and dihomo-γ-linolenic acid (DGLA, 20:3) were not observed between the two groups (Fig. 2*F*). Accordingly, the levels of PE (18:0/20:4) and PE (18:0/22:4), which are the most susceptible to oxidation upon ferroptosis induction, were increased in mesenchymal-type GCs (Fig. 2*F*) (21). Since serum also contains various PUFAs, we next addressed the ability of cells to metabolize LA using an isotope tracing analysis to distinguish it from endogenous LA (Fig. 2*C*). When cultured in [U-$^{13}C_{18}$] LA-containing medium, all cells absorbed [U-$^{13}C_{18}$] LA and metabolized it to eicosadienoic acid (EDA, C20:2). However, intestinal-type GCs, which express ELOVL5 and FADS1 at low levels, failed to synthesize DGLA (C20:3), AA (C20:4), and AdA (C22:4) from LA, whereas mesenchymal-type GCs with high levels of ELOVL5 and FADS1 produced ^{13}C-labeled DGLA and AA (Fig. 2*G*). Consequently, only mesenchymal-type GCs contained high levels

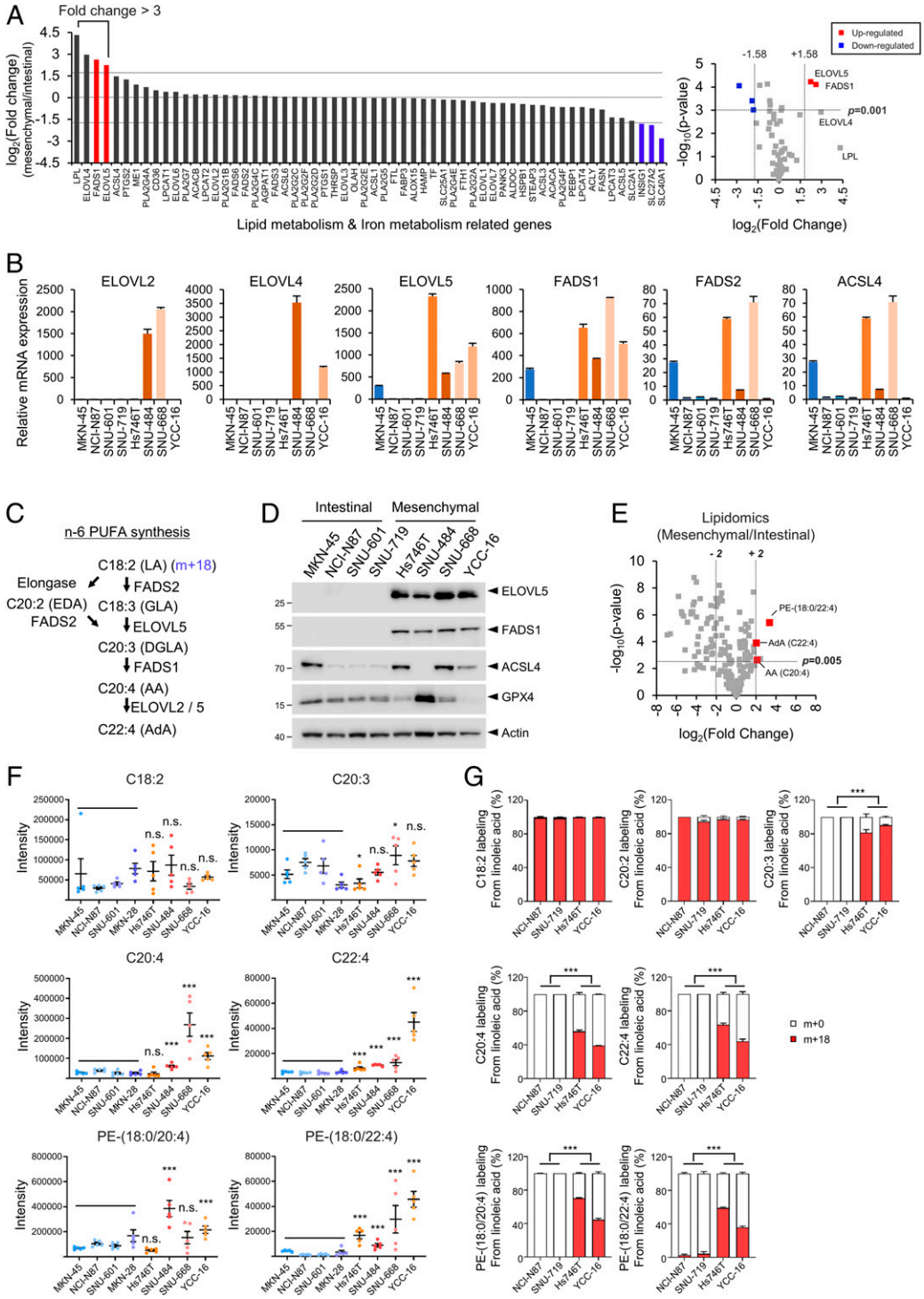

Fig. 2. ELOVL5 and FADS1 expressions are up-regulated in mesenchymal-type GCs. (*A*) Fold changes in the expression of genes associated with lipid and iron metabolism in mesenchymal-type GCs (Hs746T, SNU484, SNU-668, and YCC-16 cells) compared with intestinal-type GCs (MKN-45, NCI-N87, SNU-601, and SNU-719 cells) based on the results of a microarray analysis. Volcano plot showing fold changes and *P* values of mRNA expression levels. Significantly up-regulated or down-regulated genes (*P* value <0.001, |fold change| > 3) are shown in red or blue, respectively. (*B*) Levels of the *ELOVL2*, *ELOVL4*, *ELOVL5*, *FADS1*, *FADS2*, and *ACSL4* mRNAs in GCs were analyzed using qRT-PCR. Relative expression levels were normalized to the *β-actin* expression levels. Data are the means ± SD ($n = 3$ independent experiments). (*C*) Scheme showing the incorporation of LA into the n-6 PUFA synthesis pathway. LA, linoleic acid; GLA, gamma-linoleic acid; EDA, eicosadienoic acid; DGLA, dihomo-γ-linolenic acid; AA, arachidonic acid; AdA, adrenic acid. (*D*) Western blots showing the levels of ELOVL5, FADS1, ACSL4, and GPX4 proteins in mesenchymal- and intestinal-type GCs. For the detection of ELOVL5 protein, samples were not boiled. (*E*) Volcano plot showing fold changes and *P* values for lipid species in mesenchymal-type GCs and intestinal-type GCs. Free AA, AdA, and PE (18:0/22:4) are highlighted in red. (*F*) Levels of PUFAs and PE detected in GCs using LC-MS/MS. Intensities were normalized to the total sum of the peak areas. Data are the means ± SD ($n = 5$ independent experiments), with $^{*}P < 0.05$ and $^{***}P < 0.001$ compared to intestinal-type cells ($n = 20$) using one-sided Wilcoxon rank-sum test (n.s. denotes not significant). (*G*) Relative amounts of labeled (m + 18) and unlabeled (m + 0) PUFAs and PE in NCI-N87, SNU-719, Hs746T, and YCC-16 cells cultured in medium containing charcoal-stripped FBS and [U-$^{13}C_{18}$] LA for 5 d.

of PE (18:0/20:4) and PE (18:0/22:4) (Fig. 2*G*). Thus, the expression of ELOVL5 and FADS1 is required for the production of the ferroptosis-related phospholipids PE (18:0/20:4) and PE (18:0/22:4), which are required for ferroptosis.

The Sensitivity to Ferroptosis Is Regulated by ELOVL5 and FADS1. To ascertain whether ELOVL5 and FADS1 indeed play a key role in the ferroptotic cell death pathway, we first assessed the responses of ELOVL5- or FADS1-depleted cells. The siRNA-mediated knockdown of ELOVL5 and FADS1 prevented RSL3-induced cell death in Hs746T, SNU-484, and YCC-16 cells (*SI Appendix*, Fig. S4 *A–C*). We next measured the levels of lipid peroxidation, a hallmark of ferroptosis, using C11 BODIPY 581/591 (1, 17). ELOVL5- or FADS1-depleted cells showed decreased lipid peroxidation levels following RSL3 treatment compared with control cells (*SI Appendix*, Fig. S4 *D–F*). Moreover, ELOVL5- or FADS1-KO YCC-16 cells are highly resistant to RSL3-induced ferroptosis by suppressing lipid peroxidation (Fig. 3 *A* and *B*).

We next conducted an isotope tracing analysis in ELOVL5- and FADS1-KO cells using ^{13}C LA (C18:2) to validate whether these cells are indeed defective in the PUFA biosynthesis. Although the intestinal-type GCs expressing low levels of ELOVL5 were able to synthesize EDA (C20:2) from LA (C18:2) (Fig. 2*G*), ELOVL5-KO YCC-16 cells were unable to generate EDA (C20:2) (Fig. 3*C*), suggesting that YCC-16 cells were entirely dependent on ELOVL5 for the biosynthesis of EDA. Furthermore, FADS1-KO cells failed to synthesize AA (C20:4) from DGLA (C20:3) (Fig. 3*C*). As a result, neither ^{13}C-PE (18:0/20:4) nor ^{13}C-PE (18:0/22:4) were detected in ELOVL5- or FADS1-KO cells (Fig. 3*C*).

We performed an LC-MS/MS analysis to verify whether the resistance to ferroptosis induced by the down-regulation of ELOVL5 or FADS1 was due to reduced amounts of ferroptosis-related lipids. Deletion of ELOVL5 decreased the ratio of AdA (C22:4) to AA (C20:4), the synthesis of which is mediated by ELOVL5 (Fig. 3*D*). Similarly, FADS1-KO cells exhibited significant decreases in the ratios of AA (C20:4) to DGLA (C20:3) (Fig. 3*D*). However, cells deficient in ELOVL5 and FADS1 contained comparable amounts of DGLA (C20:3) and AA (C20:4) to wild-type (WT) cells, while the levels of AdA (C22:4) in ELOVL5-KO cells were markedly lower than those in WT cells (Fig. 3*D*). These observations imply that DGLA (C20:3) and AA (C20:4), but not AdA (C22:4), can be supplied to these cells from the extracellular environment (Fig. 3*D*). Eventually, the levels of AdA and PE (18:0/22:4) were significantly reduced in ELOVL5-deleted cells, while those of AA and PE (18:0/20:4) were decreased in FADS1-deleted cells (Fig. 3*D*). Consistently, depletion of ELOVL5 or FADS1 drastically decreased the ratios of AdA (C22:4) to AA (C20:4) and AA (C20:4) to DGLA (C20:3) (*SI Appendix*, Fig. S4 *G* and *H*). Eventually, ELOVL5- or FADS1-depleted cells contained lower levels of AA, AdA, PE (18:0/20:4), and PE (18:0/22:4) (*SI Appendix*, Fig. S4 *G* and *H*). In particular, we observed only subtle differences in the levels of AA (C20:4) and PE (18:0/20:4) between control and siRNA-transfected cells (*SI Appendix*, Fig. S4 *G* and *H*). Because more significant differences in AdA and PE (18:0/22:4) levels than in AA (C20:4) and PE (18:0/20:4) levels were observed between mesenchymal-type and intestinal-type GCs (Fig. 2*F*), PE (18:0/22:4) might be more crucial in the induction of ferroptosis in GCs. Nevertheless, down-regulation of ELOVL5 or FADS1 lowers

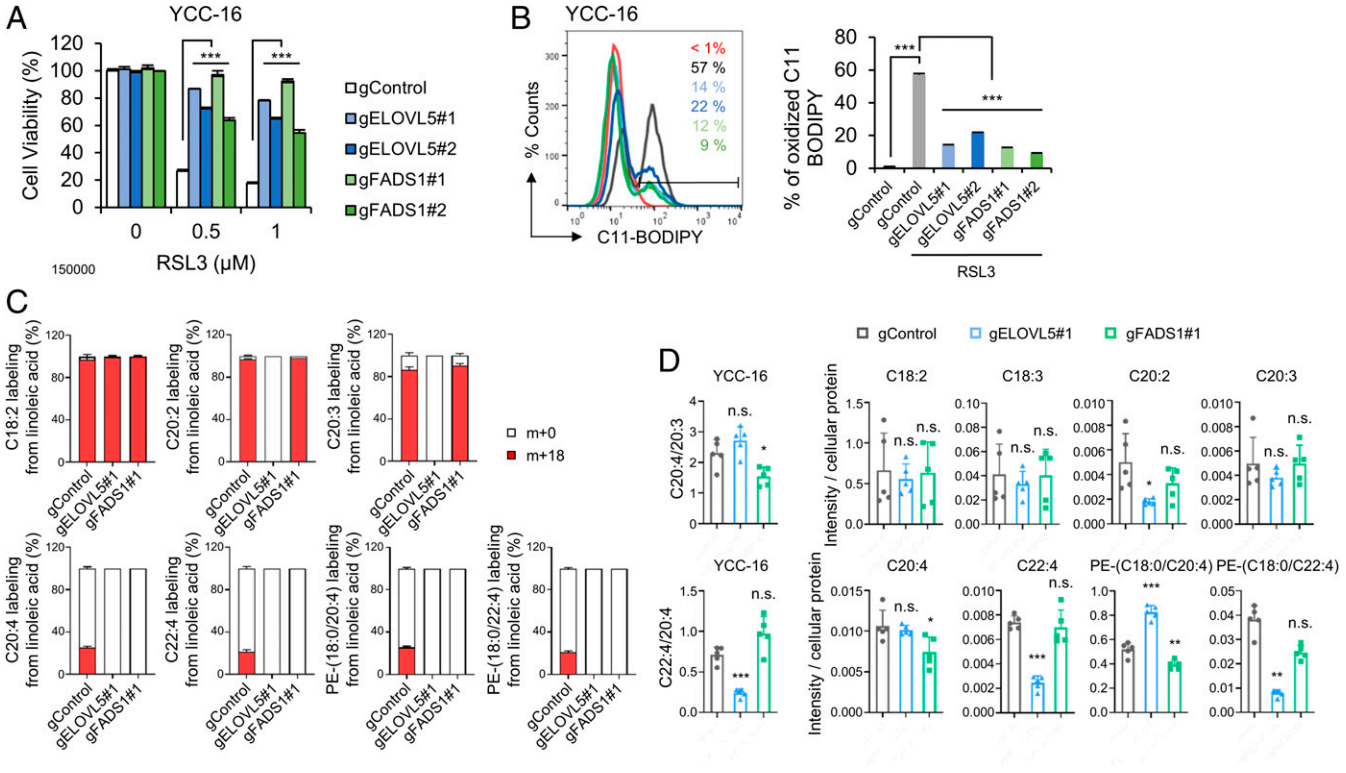

Fig. 3. The down-regulation of ELOVL5 and FADS1 expression alleviates ferroptosis. (*A* and *B*) Relative viability and lipid peroxidation levels in WT, ELOVL5-, and FADS1-KO YCC-16 cells treated with RSL3. Data are the means ± SD ($n = 3$ independent experiments, with $^{***}P < 0.001$ according to two-sided Student's *t* tests). (*C*) Relative amounts of labeled (m + 18) and unlabeled (m + 0) PUFAs and PE in WT, ELOVL5-, and FADS1-KO YCC-16 cells cultured in medium containing charcoal-stripped FBS and [U-$^{13}C_{18}$] LA. (*D*) Bar plots showing the ratios of AdA (C22:4) to AA (C20:4) and AA (C20:4) to DGLA (C20:3) in ELOVL5- and FADS1-KO YCC-16 cells. Levels of PUFAs and PE in ELOVL5- and FADS1-KO YCC-16 cells determined using LC-MS/MS. Intensities were normalized to the cellular protein level. Data are the means ± SD ($n = 5$ independent experiments), with $^{*}P < 0.05$, $^{**}P < 0.01$ and $^{***}P < 0.001$ according to a two-sided Student's test (n.s. denotes not significant).

the levels of ferroptosis-related lipids such as PE (18:0/20:4) and PE (18:0/22:4) and inhibits ferroptosis, suggesting crucial roles for ELOVL5 and FADS1 in maintaining the intracellular pool of PUFAs and their PE-linked species, which are indispensable for ferroptosis sensitization.

We next employed SC-26196, a selective FADS2 inhibitor, and CP-24879, a FADS1/FADS2 dual inhibitor. Since several inhibitors often possess intrinsic antioxidant activity, we first measured the scavenging capacity of FADS inhibitors toward 2,2-diphenyl-1-picrylhydrazyl (DPPH) under cell-free conditions (30). Similar to the results of a previous report, ferrostatin-1 showed free radical scavenging activity at concentrations of 10 to 50 μM under our experimental conditions (31). While SC-26196 displayed no antioxidant potential, high concentrations of CP-24879 scavenged 60% of the DPPH radical within 30 min (*SI Appendix*, Fig. S5). To exclude the antioxidant effect of CP-24879, inhibitors were used at a low concentration (5 μM) with no in vitro antioxidant activity in subsequent experiments. The inhibition of desaturase activity by the SC-26196 or CP-24879 treatment dramatically reduced the cytotoxicity induced by RSL3 (Fig. 4 *A* and *B*). Furthermore, RSL3-induced lipid peroxidation was noticeably decreased in the presence of SC-26196 or CP-24879 (Fig. 4*C*). We next assessed whether the PUFA biosynthesis pathway was also required for ferroptosis under GSH depletion conditions. First, cysteine/methionine deprivation-induced ferroptosis was ameliorated in ELOVL5- or FADS1-depleted cells (Fig. 4*D*). In addition, SC-26196 or CP-24879 suppressed cell death under cysteine/methionine deprivation conditions (Fig. 4*E*). Based on these data, PUFA biosynthesis enzymes play essential roles in lipid peroxidation and ferroptosis.

AA Supplementation Renders Intestinal-Type GCs Sensitive to Ferroptosis. Since intestinal-type GCs contain reduced amounts of AA and AdA, possibly due to the reduced levels of ELOVL5 and FADS1, we hypothesized that exogenous PUFAs might promote ferroptosis. The treatment of intestinal-type NCI-N87 and SNU-719 cells with AA markedly increased their sensitivity to ferroptosis, with an increase in the levels of PE (18:0/20:4) (Fig. 5 *B* and *C*). AA also further promoted the death of mesenchymal-type Hs746T and SNU-484 cells, suggesting that an increase in intracellular AA levels might accelerate cell death, even in ferroptosis-sensitive cells (Fig. 5*A*). In addition, deuterated AA (AA-d8), which was shown to be oxidized and sensitizes cells to ferroptosis (21), also substantially increased the ferroptosis sensitivity of intestinal-type cells (*SI Appendix*, Fig. S6 *A* and *B*). Interestingly, although NCI-N87 cells treated with LA or the vehicle control did not exhibit lipid peroxidation in response to RSL3 treatment, cells supplemented with AA or AA-d8 exhibited increased lipid peroxidation in response to RSL3 (Fig. 5*D* and *SI Appendix*, Fig. S6*C*). Thus, AA, but not the general AA biosynthesis pathway, was required for ferroptosis. Furthermore, AA supplementation induced ferroptosis in response to RSL3 treatment or cysteine/methionine deprivation (Fig. 5 *E–H* and *SI Appendix*, Fig. S6 *D* and *E*). Our data imply that intracellular AA levels are the key determinant of ferroptosis.

ELOVL5 and FADS1 Are Frequently Silenced in Intestinal-Type GCs with Increased DNA Methylation at Promoter/Enhancer Regions. We next investigated *ELOVL5* and *FADS1* expression in other types of cancers using public gene expression data available from the Project Achilles dataset and the Cancer Cell Line Encyclopedia (CCLE) (32–35). Levels of *ELOVL5* and *FADS1* mRNAs were

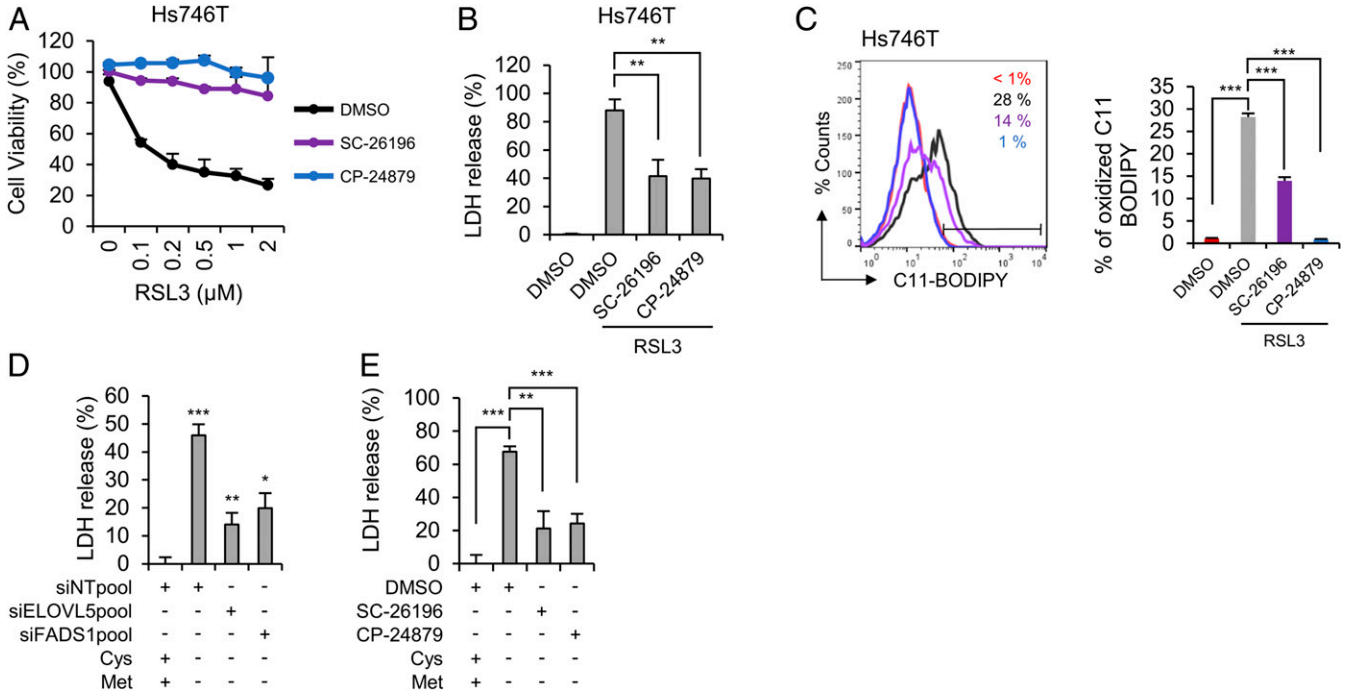

Fig. 4. Inhibition of desaturase activity by SC-26196 or CP-24879 ameliorates ferroptosis. (*A* and *B*) Relative cell viability and LDH levels in Hs746T cells pretreated with 5 μM FADS2 inhibitor (SC-26196) or FADS1/2 inhibitor (CP-24879) for 4 h and treated with RSL3 for 24 h. Data are the means ± SD ($n = 3$ independent experiments, with $^{**}P < 0.01$ according to two-sided Student's *t* tests). (*C*) Lipid peroxidation levels in Hs746T cells pretreated with 5 μM FADS2 inhibitor (SC-26196) or FADS1/2 inhibitor (CP-24879) for 4 h and treated with RSL3 for 1 h. Data are the means ± SD ($n = 3$ independent experiments, with $^{***}P < 0.001$ according to two-sided Student's *t* tests). (*D*) Cell death determined by LDH release from ELOVL5- or FADS1-depleted Hs746T cells cultured in cysteine/methionine-deficient medium for 24 h. Data are the means ± SD ($n = 3$ independent experiments, with $^{*}P < 0.05$, $^{**}P < 0.01$ and $^{***}P < 0.001$ according to two-sided Student's *t* tests). (*E*) Cell death measured by LDH release from Hs746T cells pretreated with FADS inhibitors for 4 h, followed by an incubation with cysteine/methionine-deficient medium for 24 h. Data are the means ± SD ($n = 3$ independent experiments, with $^{**}P < 0.01$ and $^{***}P < 0.001$ according to two-sided Student's *t* tests).

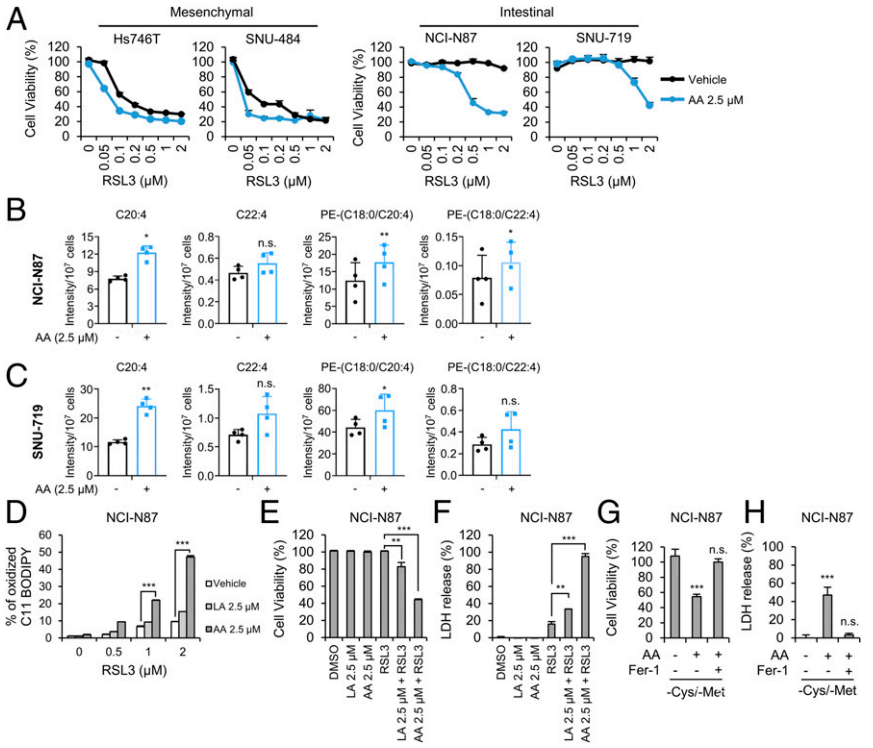

Fig. 5. Exogenous AA supplementation restores the sensitivity of intestinal-type GCs to ferroptosis. (*A*) Relative viability of GCs pretreated with 2.5 μM of AA for 16 h and treated with RSL3 for 24 h. Data are the means ± SD ($n = 3$ independent experiments). (*B* and *C*) Levels of the indicated lipids in NCI-N87 and SNU-719 cells treated with 2.5 μM AA for 3 h determined using LC-MS/MS. Intensities were normalized to cell numbers. Data are the means ± SD ($n = 4$ independent experiments), with $^{*}P < 0.05$, and $^{**}P < 0.01$ according to two-sided Student's tests (n.s. denotes not significant). (*D*) Lipid peroxidation levels in NCI-N87 cells pretreated with 2.5 μM PUFAs for 16 h and treated with RSL3 for 1 h. Data are the means ± SD ($n = 3$ independent experiments), with $^{***}P < 0.001$ according to two-sided Student's tests. (*E* and *F*) Cell viability and cell death as measured by LDH release from NCI-N87 cells pretreated with LA and AA for 16 h and treated with RSL3 for 24 h. Data are the means ± SD ($n = 3$ independent experiments), with $^{**}P < 0.01$ and $^{***}P < 0.001$ according to two-sided Student's tests. (*G* and *H*) Cell viability of and LDH release from NCI-N87 cells cultured with cysteine/methionine-deficient medium in the presence and absence of AA and Fer-1. Data are the means ± SD ($n = 3$ independent experiments, n.s. denotes not significant, $^{***}P < 0.001$ according to two-sided Student's *t* tests).

generally increased in most types of cancer (*SI Appendix*, Fig. S7 *A* and *B*). Strikingly, *ELOVL5* and *FADS1* were broadly distributed in several types of cancer, such as gastric and colorectal cancer (*SI Appendix*, Fig. S7 *A* and *B*). Therefore, ELOVL5 and FADS1 essentially function in long-chain PUFA production in most cells, but some types of cells might lose ELOVL5 and FADS1 expression. Since DNA methylation is often associated with gene silencing, we investigated the correlation between gene expression and DNA methylation using the CCLE database. Consistent with the mRNA expression data, the DNA methylation levels were low in most types of cancer, whereas a subset of gastric and colorectal cancer cells exhibited high levels of methylation (*SI Appendix*, Fig. S7 *A* and *B*). As confirmation of these findings, *ELOVL5* and *FADS1* expression levels were inversely correlated with DNA methylation in all types of cancer cells, suggesting that the expression of these genes was primarily regulated by DNA methylation (*SI Appendix*, Fig. S7 *A* and *B*).

To further closely monitor the DNA methylation at the promoter regions of *ELOVL5* and *FADS1*, we performed a methylation sequencing analysis using mesenchymal- and intestinal-type GCs to detect each type of CpG methylation. Consistent with the results obtained from the CCLE database, the promoter region of *ELOVL5* in intestinal-type GCs exhibited significantly higher levels of methylation than in mesenchymal-type GCs (Fig. 6 *A* and *B*). The *FADS1* and *FADS2* genes are located in different directions on the same locus of the chromosome, and their expression is often simultaneously regulated (36, 37). Interestingly, DNA methylation was mostly detected in the first exon and intron of *FADS1* rather than at its promoter or enhancer region in intestinal-type GCs (Fig. 6 *A* and *B*). DNA methylation around the *FADS2* promoter was also observed, but the difference between mesenchymal- and intestinal-type GCs was less significant (Fig. 6*B*). In addition, methylation around the *FADS2* promoter was not correlated with the mRNA expression levels (Fig. 6*B*). Collectively, intestinal-type GCs display hypermethylation around the promoter regions of *ELOVL5* and *FADS1*, resulting in the low levels of ELOVL5 and FADS1 expression and eventually contributing to ferroptosis resistance.

Discussion

A previous study identified AA and AdA anchored in phosphatidylethanolamine as the primary targets of LOXs, and therefore, these species are essential components for ferroptosis (21, 22). In this regard, ACSL4, which links AA and AdA to PE, has been suggested to be an essential factor in many studies (21, 38–40). In particular, ACSL4 is expressed at high levels in basal-type breast cancer cells, which are sensitive to ferroptosis, whereas it is often silenced in luminal-type breast cancer cells, leading to ferroptosis resistance (21). Consistent with these findings, the CCLE database revealed high *ACSL4* expression in most types of cancer, while its expression varies in breast cancer cells (*SI Appendix*, Fig. S7*C*). Unlike *ACSL4*, *ELOVL5* and *FADS1* are expressed at high levels in most cancer cells, but several types of cancer, including gastric and colorectal cancer, often exhibit low expression levels of these enzymes. In

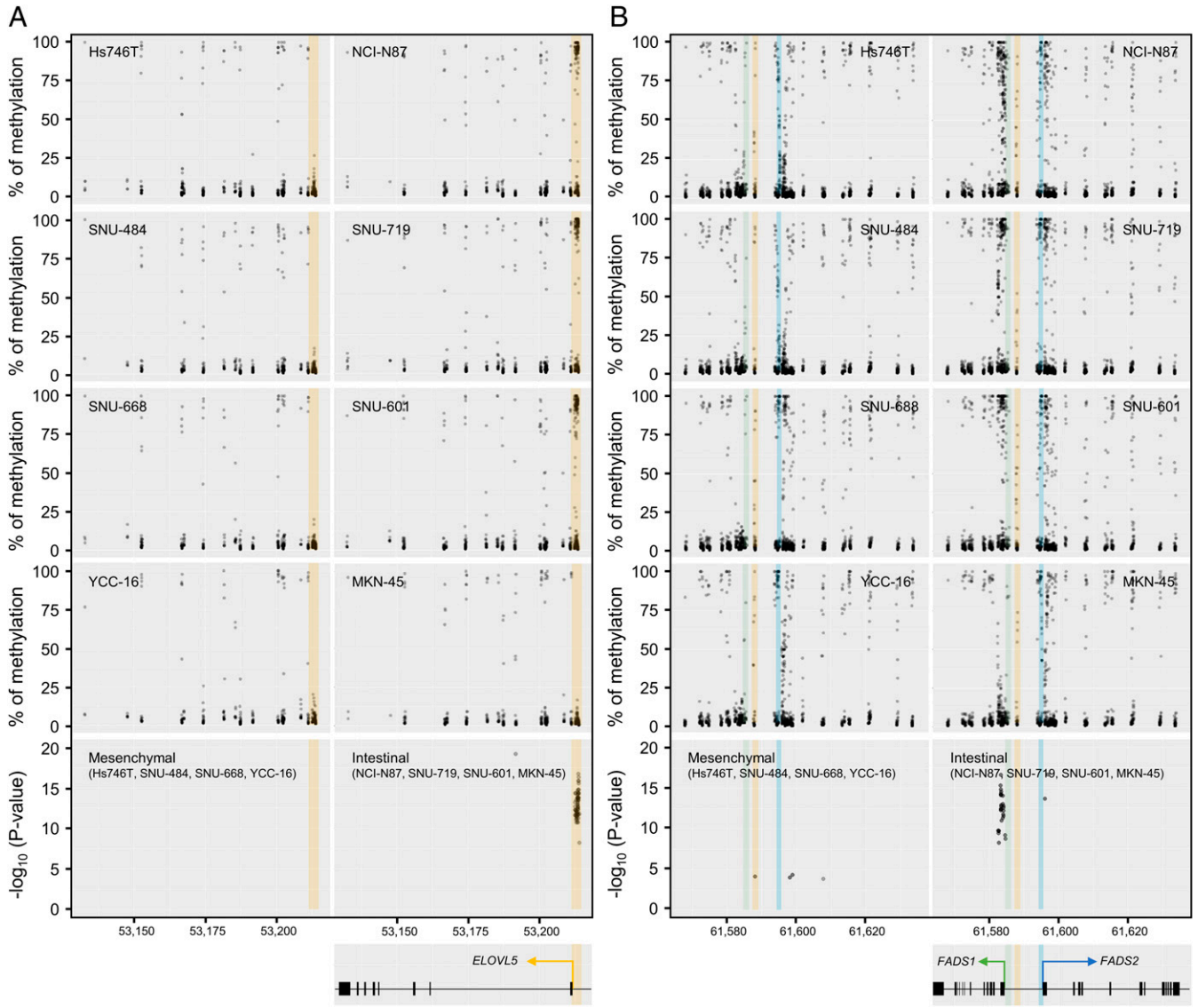

Fig. 6. *ELOVL5* and *FADS1* expression is down-regulated through DNA hypermethylation. (*A* and *B*) Manhattan plot of the methylation levels and statistical significance of methylation at each CpG site in the promoter regions of *ELOVL5* (*A*) and *FADS1*/*2* (*B*) in mesenchymal-type (Hs746T, SNU484, SNU-668, and YCC-16) and intestinal-type (NCI-N87, SNU-719, SNU-601, and MKN-45) GCs. The putative enhancer/promoter region of *ELOVL5* (chr6: 53,211,316 to 53,214,820) is highlighted in orange. The putative regions of the *FADS1* promoter (chr11: 61,584,650 to 61,586,300), *FADS2* promoter (chr11: 61,594,300 to 61,595,600) and putative enhancer (chr11: 61,587,300 to 61,589,000) are colored in green, blue, and orange, respectively (36).

particular, most intestinal-type GCs express *ELOVL5* and *FADS1* at very low levels and contain lower levels of AA and AdA than mesenchymal-type GCs. Consequently, intestinal-type GCs are less sensitive to ferroptosis than mesenchymal-type GCs, but the ferroptosis sensitivity of these cells is increased by supplementation with AA. In addition, low expression of *ELOVL5* and *FADS1* is associated with an increase in DNA methylation around their promoter regions. Notably, *ACSL4* expression varies across all cancers, and DNA methylation levels are generally low. Furthermore, we did not observe a correlation between expression and methylation, suggesting that *ACSL4* might not be regulated by promoter methylation (*SI Appendix*, Fig. S7*C*). Based on these data, ELOVL5 and FADS1 are unique enzymes that differ from ACSL4 in terms of their regulatory mechanism. Interestingly, MKN-45 cells express ELOVL5 and FADS1 proteins at very low levels, despite their comparable mRNA expression levels, suggesting the possible existence of a posttranslational mechanism regulating the expression of these proteins (*SI Appendix*, Fig. S2*A*). In addition, the expression of several enzymes involved in lipid metabolism is up-regulated in some mesenchymal-type GCs (Fig. 2 *A* and *B*). Among these enzymes, ELOVL4, which mediates the elongation of very long-chain PUFAs such as C26:5 and C26:6, is overexpressed in SNU-484 and YCC-16 cells, but the role of these PUFAs in ferroptosis has not been studied. Although ELOVL4 knockdown did not exert an effect on SNU-484 and Hs746T cells, the depletion of ELOVL4 significantly reduced RSL3-induced ferroptosis and lipid peroxidation in YCC-16 cells (*SI Appendix*, Fig. S8 *A*–*D*). Thus, very long-chain PUFAs might positively affect ferroptosis in a context-dependent manner, and further investigations are required to confirm these hypotheses in the future.

Although we focused on the PUFA biosynthesis pathway in this study, exogenous AA supplementation in intestinal-type GCs did not completely reverse the sensitivity to ferroptosis

compared with mesenchymal-type GCs. Therefore, other factors may discriminate the sensitivity of mesenchymal- and intestinal-type GCs to ferroptosis. In addition to PUFA biosynthesis, AA and AdA transport might be important contributors to ferroptosis sensitivity, since cells are able to directly take up AA and AdA. Our microarray data showed no significant difference in the expression levels of fatty acid transporters such as CD36 (FAT) and SLC27A1 (FATP1) between the two groups (Datasets S2 and S3) (41). In particular, significantly lower levels of SLC27A2 (FATP2), another fatty acid transporter which is crucial for AA uptake, were detected in mesenchymal-type GCs than in intestinal-type GCs (Datasets S2 and S3) (42). Therefore, the intracellular synthesis of AA might be predominately used for lipid peroxidation rather than AA import, because intestinal-type GCs are resistant to ferroptosis despite the presence of AA in the fetal bovine serum (FBS)-containing medium. In addition, the expression of SLC40A1, also known as ferroportin (FPN1), which exports iron from cells (43), is significantly down-regulated in mesenchymal-type GCs compared with intestinal-type GCs. Since SLC40A1 negatively regulates ferroptosis by reducing intracellular iron levels (43–45), the increased activity of SLC40A1 in intestinal-type GCs might contribute to ferroptosis resistance. Finally, we found that the up-regulation of the expression of target genes in the NRF2 pathway, a master antioxidant transcription factor, in intestinal-type GCs compared with mesenchymal-type GCs. Since NRF2 protects cells from ferroptosis in various types of tissues and cancers (12, 46, 47), the NRF2-dependent antioxidant pathway may further repress ferroptosis in intestinal-type GCs. Collectively, these results indicate that various pathways, such as lipid metabolism, iron metabolism, the general antioxidant pathway, and other pathways, cooperatively function in each cell type to control ferroptosis sensitivity. Among these pathways, the expression of PUFA-related enzymes might be lost in several cell types, leading to ferroptosis resistance. Therefore, the expression of these enzymes will be potentially useful as a predictive marker in the future. Given the critical roles of ferroptosis in several human diseases, such as I/R injury, the PUFA biosynthesis pathway might be a potential target for the treatment of related diseases.

Materials and Methods

Cysteine/Methionine Deprivation. For cysteine/methionine deprivation, cysteine-free Dulbecco's modified Eagle's medium (DMEM, lacking glutamine, methionine, and cysteine; 21013024, Gibco) supplemented with 10% dialyzed FBS (26400044; Gibco) and 2 mM L-glutamine (Gibco) was used. Cells were washed with phosphate-buffered saline (PBS) and cultured with fresh DMEM or cysteine-free DMEM for 24 h in the presence or absence of Fer-1.

Chemicals. RSL3 (S8155), ferrostatin-1 (Fer-1, S7243), and zVAD-fmk (zVAD, S7023) were purchased from Selleck Chemicals. Liproxstatin-1 (Lip-1, SML1414), ML210 (SML0521), CP-24879 (C9115), and SC-26196 (PZ0176) were purchased from Sigma-Aldrich. Necrostatin-1 (Nec-1, BML-AP309) was purchased from Enzo Life Sciences. C11 BODIPY 581/591 (D3861) was obtained from Molecular Probes and dissolved in dimethyl sulfoxide (DMSO). LA (90150), AA (90010), and AA-d8 (390010) were purchased from Cayman Chemical. All chemicals were stored at −20 °C, except CP-24879, which was stored at room temperature until use.

Western Blotting Analysis. Western blot analyses were performed using previously described methods (48). Cells were lysed in lysis buffer (50 mM Tris·HCl pH 7.5, 150 mM NaCl, 0.5% Nonidet P-40, 0.5% Triton X-100, 0.1% Na-deoxycholate, and 1 mM ethylenediaminetetraacetic acid containing a protease inhibitor mixture). The whole-cell extracts were subjected to Western blot analysis using the following antibodies: anti-β-actin (A5316, Sigma-Aldrich), anti-FADS1 (HPA042705, Atlas Antibodies; ab126706, Abcam; sc-134337, Santa Cruz Biotechnology; GTX114528, Genetex; 10627-1-AP, Proteintech), anti-ELOVL5 (ab205535, Abcam; sc-374138, Santa Cruz Biotechnology), anti-GPX4 (ab41789, Abcam), and anti-ACSL4 (sc-271800, Santa Cruz Biotechnology). For detection of ELOVL5 protein, samples were not boiled.

Isotope Labeling and Tracing Analysis Using LC-MS/MS. The [U-$^{13}C_{18}$] LA was purchased from Sigma-Aldrich. Stable isotope labeling in cells was accomplished by culturing cells in tracer medium supplemented with isotopic LA (100 μM) and 10% charcoal-stripped FBS for 5 d. The lipids were extracted in 400 μL of a 40:40:20 acetonitrile:methanol:water solution containing a 0.5% formic acid solution. The extracts were cleared by centrifugation, and the lipids in the supernatant were directly analyzed using ultra-performance liquid chromatography-triple-quadrupole mass spectrometry (UPLC-TQ-MS) in multiple reaction monitoring (MRM) mode. An Agilent 1290 Infinity II LC and Agilent 6495 Triple Quadrupole MS system equipped with an Agilent Jet Stream ESI source (Agilent Technologies) was used for the analysis. MassHunter Workstation (ver. B.06.00, Agilent Technologies) software was used for data acquisition and analysis. Chromatographic separation was performed using an Acquity UPLC BEH C18 column (2.1 mm × 100 mm, 1.7 μm; Waters) at 30 °C; binary gradient separation was performed at a flow rate of 0.2 mL/min. The injection volume was 10 μL. The mobile phases consisted of 10 mM ammonium acetate in water:acetonitrile (60:40 vol/vol, solvent A) and 10 mM ammonium acetate in isopropanol:acetonitrile (90:10 vol/vol, solvent B). The steps of the gradient profile used to equilibrate the initial gradient for subsequent runs were 40 to 55% B from 0 to 6 min, 55 to 60% B from 6 to 11 min, 60 to 99% B from 11 to 14 min, 99% B from 14 to 18 min, 99 to 40% B from 18 to 18.1 min, and 40% B from 18.1 to 21 min. The MS system was operated using the following parameter settings: gas temperature of 220 °C, nebulizer gas of nitrogen at 30 psi, sheath gas temperature of 300 °C, and sheath gas flow rate of 11 L/min.

Statistical Analysis. All experiments were performed at least in triplicate. All data are presented as means ± SD. The statistical significance of differences between two groups was measured using two-tailed Student's *t* tests or the Wilcoxon rank-sum test. Statistical analyses were performed using Prism 8 software (GraphPad Software), and differences were considered significant at $P < 0.05$.

Data Availability. All study data are included in the article and supporting information.

ACKNOWLEDGMENTS. We thank Dr. Kyung-Min Noh for providing the pSpCas9(BB)-2A-RFP plasmid. This study was supported by grants from the KRIBB Research Initiative Program, the Korea Basic Science Institute (C060200), the Development of Measurement Standards and Technology for Biomaterials and Medical Convergence funded by the Korea Research Institute of Standards and Science (KRISS–2020–GP2020-0004), and the National Research Foundation of Korea (NRF) funded by the Ministry of Science and ICT and Future Planning (NRF-2015M3A9D7029882, NRF-2017M3A9G5083321, NRF-2017M3A9G5083322, 2019M3A9D5A01102796, NRF-2019R1C1C1002831, and NRF-2020R1A2C2007835).

1. S. J. Dixon *et al.*, Ferroptosis: An iron-dependent form of nonapoptotic cell death. *Cell* **149**, 1060–1072 (2012).
2. A. Seiler *et al.*, Glutathione peroxidase 4 senses and translates oxidative stress into 12/15-lipoxygenase dependent- and AIF-mediated cell death. *Cell Metab.* **8**, 237–248 (2008).
3. J. Li *et al.*, Ferroptosis: Past, present and future. *Cell Death Dis.* **11**, 88 (2020).
4. L. Galluzzi *et al.*, Molecular mechanisms of cell death: Recommendations of the nomenclature committee on cell death 2018. *Cell Death Differ.* **25**, 486–541 (2018).
5. B. Hassannia, P. Vandenabeele, T. Vanden Berghe, Targeting ferroptosis to iron out cancer. *Cancer Cell* **35**, 830–849 (2019).
6. B. R. Stockwell *et al.*, Ferroptosis: A regulated cell death nexus linking metabolism, redox biology, and disease. *Cell* **171**, 273–285 (2017).
7. J. P. Friedmann Angeli *et al.*, Inactivation of the ferroptosis regulator Gpx4 triggers acute renal failure in mice. *Nat. Cell Biol.* **16**, 1180–1191 (2014).
8. A. Linkermann *et al.*, Synchronized renal tubular cell death involves ferroptosis. *Proc. Natl. Acad. Sci. U.S.A.* **111**, 16836–16841 (2014).
9. X. Fang *et al.*, Ferroptosis as a target for protection against cardiomyopathy. *Proc. Natl. Acad. Sci. U.S.A.* **116**, 2672–2680 (2019).
10. S. J. Dixon *et al.*, Pharmacological inhibition of cystine-glutamate exchange induces endoplasmic reticulum stress and ferroptosis. *eLife* **3**, e02523 (2014).
11. C. Louandre *et al.*, Iron-dependent cell death of hepatocellular carcinoma cells exposed to sorafenib. *Int. J. Cancer* **133**, 1732–1742 (2013).
12. X. Sun *et al.*, Activation of the p62-Keap1-NRF2 pathway protects against ferroptosis in hepatocellular carcinoma cells. *Hepatology* **63**, 173–184 (2016).
13. M. Hayano, W. S. Yang, C. K. Corn, N. C. Pagano, B. R. Stockwell, Loss of cysteinyl-tRNA synthetase (CARS) induces the transsulfuration pathway and inhibits ferroptosis induced by cystine deprivation. *Cell Death Differ.* **23**, 270–278 (2016).

14. L. Wang *et al*., A pharmacological probe identifies cystathionine β-synthase as a new negative regulator for ferroptosis. *Cell Death Dis.* **9**, 1005 (2018).
15. J. Zhu *et al*., Transsulfuration activity can support cell growth upon extracellular cysteine limitation. *Cell Metab.* **30**, 865–876.e5 (2019).
16. M. Weïwer *et al*., Development of small-molecule probes that selectively kill cells induced to express mutant RAS. *Bioorg. Med. Chem. Lett.* **22**, 1822–1826 (2012).
17. W. S. Yang *et al*., Regulation of ferroptotic cancer cell death by GPX4. *Cell* **156**, 317–331 (2014).
18. M. Gao *et al*., Role of mitochondria in ferroptosis. *Mol. Cell* **73**, 354–363.e3 (2019).
19. M. J. Hangauer *et al*., Drug-tolerant persister cancer cells are vulnerable to GPX4 inhibition. *Nature* **551**, 247–250 (2017).
20. V. S. Viswanathan *et al*., Dependency of a therapy-resistant state of cancer cells on a lipid peroxidase pathway. *Nature* **547**, 453–457 (2017).
21. S. Doll *et al*., ACSL4 dictates ferroptosis sensitivity by shaping cellular lipid composition. *Nat. Chem. Biol.* **13**, 91–98 (2017).
22. S. E. Wenzel *et al*., PEBP1 wardens ferroptosis by enabling lipoxygenase generation of lipid death signals. *Cell* **171**, 628–641.e26 (2017).
23. C. Yoon *et al*., Chemotherapy resistance in diffuse-type gastric adenocarcinoma is mediated by RhoA activation in cancer stem-like cells. *Clin. Cancer Res.* **22**, 971–983 (2016).
24. J.-H. Cheong *et al*., Predictive test for chemotherapy response in resectable gastric cancer: A multi-cohort, retrospective analysis. *Lancet Oncol.* **19**, 629–638 (2018).
25. S. C. Oh *et al*., Clinical and genomic landscape of gastric cancer with a mesenchymal phenotype. *Nat. Commun.* **9**, 1777 (2018).
26. K. Yoshihara *et al*., Inferring tumour purity and stromal and immune cell admixture from expression data. *Nat. Commun.* **4**, 2612 (2013).
27. T.-J. Park *et al*., Quantitative proteomic analyses reveal that GPX4 downregulation during myocardial infarction contributes to ferroptosis in cardiomyocytes. *Cell Death Dis.* **10**, 835 (2019).
28. M. Gao, P. Monian, N. Quadri, R. Ramasamy, X. Jiang, Glutaminolysis and transferrin regulate ferroptosis. *Mol. Cell* **59**, 298–308 (2015).
29. M. Tsachaki *et al*., Impact of 17β-HSD12, the 3-ketoacyl-CoA reductase of long-chain fatty acid synthesis, on breast cancer cell proliferation and migration. *Cell. Mol. Life Sci.* **77**, 1153–1175 (2020).
30. M. Conrad, D. A. Pratt, The chemical basis of ferroptosis. *Nat. Chem. Biol.* **15**, 1137–1147 (2019).
31. R. Skouta *et al*., Ferrostatins inhibit oxidative lipid damage and cell death in diverse disease models. *J. Am. Chem. Soc.* **136**, 4551–4556 (2014).
32. J. Barretina *et al*., The cancer cell line encyclopedia enables predictive modelling of anticancer drug sensitivity. *Nature* **483**, 603–607 (2012).
33. G. S. Cowley *et al*., Parallel genome-scale loss of function screens in 216 cancer cell lines for the identification of context-specific genetic dependencies. *Sci. Data* **1**, 140035 (2014).Corrected in: *Sci. Data* **1**, 140044 (2014).
34. S. L. Schreiber *et al*.; Cancer Target Discovery and Development Network, Towards patient-based cancer therapeutics. *Nat. Biotechnol.* **28**, 904–906 (2010).
35. H. W. Cheung *et al*., Systematic investigation of genetic vulnerabilities across cancer cell lines reveals lineage-specific dependencies in ovarian cancer. *Proc. Natl. Acad. Sci. U.S.A.* **108**, 12372–12377 (2011).
36. E. Rahbar *et al*., Uncovering the DNA methylation landscape in key regulatory regions within the FADS cluster. *PLoS One* **12**, e0180903 (2017).
37. L. Schaeffer *et al*., Common genetic variants of the FADS1 FADS2 gene cluster and their reconstructed haplotypes are associated with the fatty acid composition in phospholipids. *Hum. Mol. Genet.* **15**, 1745–1756 (2006).
38. S. J. Dixon *et al*., Human haploid cell genetics reveals roles for lipid metabolism genes in nonapoptotic cell death. *ACS Chem. Biol.* **10**, 1604–1609 (2015).
39. H. Yuan, X. Li, X. Zhang, R. Kang, D. Tang, Identification of ACSL4 as a biomarker and contributor of ferroptosis. *Biochem. Biophys. Res. Commun.* **478**, 1338–1343 (2016).
40. L. Tesfay *et al*., Steroyl-CoA Desaturase 1 (SCD1) protects ovarian cancer cells from ferroptotic cell death. *Cancer Res.* **79**, 5355–5366 (2019).
41. M. J. Watt *et al*., Suppressing fatty acid uptake has therapeutic effects in preclinical models of prostate cancer. *Sci. Transl. Med.* **11**, eaau5758 (2019).
42. F. Veglia *et al*., Fatty acid transport protein 2 reprograms neutrophils in cancer. *Nature* **569**, 73–78 (2019).
43. H. Nishizawa *et al*., Ferroptosis is controlled by the coordinated transcriptional regulation of glutathione and labile iron metabolism by the transcription factor BACH1. *J. Biol. Chem.* **295**, 69–82 (2020).
44. J. Wu *et al*., Publisher Correction: Intercellular interaction dictates cancer cell ferroptosis via NF2-YAP signalling. *Nature* **572**, E20 (2019).
45. E. Panzilius *et al*, Cell density-dependent ferroptosis in breast cancer is induced by accumulation of polyunsaturated fatty acid-enriched triacylglycerides. *bioRxiv*: 10.1101/417949 (1 October 2019).
46. Z. Fan *et al*., Nrf2-Keap1 pathway promotes cell proliferation and diminishes ferroptosis. *Oncogenesis* **6**, e371 (2017).
47. J. L. Roh, E. H. Kim, H. Jang, D. Shin, Nrf2 inhibition reverses the resistance of cisplatin-resistant head and neck cancer cells to artesunate-induced ferroptosis. *Redox Biol.* **11**, 254–262 (2017).
48. H.-Y. Yun *et al*., Structural basis for recognition of the tumor suppressor protein PTPN14 by the oncoprotein E7 of human papillomavirus. *PLoS Biol.* **17**, e3000367 (2019).